Low-Density Plasmas Below the Optical Breakdown Threshold - Potential Hazard for Multiphoton Microscopy, and a Tool for the Manipulation of Intracellular Events

Alfred Vogel[1*], Joachim Noack[1§], Gereon Hüttmann[1], and Günther Paltauf [2]

1) Medizinisches Laserzentrum Lübeck, 23562 Lübeck, Germany
2) Department of Applied Physics, Karl-Franzens-Universität, 8010 Graz, Austria

ABSTRACT

Irradiance values employed in multiphoton microscopy are only one order of magnitude below the irradiance threshold for femtosecond optical breakdown in aqueous media ($\approx 1.0 \times 10^{13}$ W cm^{-2}). At the breakdown threshold, a plasma with a free electron density of about 10^{21} cm^{-3} is generated, and the energy density in the breakdown region is sufficiently high to cause the formation of a bubble at the laser focus. We found previously that plasmas with a free electron density $<10^{21}$ cm^{-3} are formed also in a fairly large irradiance range below the breakdown threshold. The present study investigates the chemical, thermal, and thermomechanical effects produced by these low-density plasmas, and their consequences for multiphoton microscopy. We use a rate equation model considering multiphoton ionization and avalanche ionization to numerically simulate the plasma formation. The value of the plasma energy density created by each laser pulse is then used to calculate the temperature distribution in the focal region. The results of the temperature calculations yield, finally, the starting point for calculations of the thermoelastic stresses that are generated during the formation of the low-density plasmas.

We found that with femtosecond pulses a large 'tuning range' exists for the creation of spatially extremely confined chemical, thermal and mechanical effects via free electron generation through nonlinear absorption. Photochemical effects dominate at the lower end of this irradiance range, whereas at the upper end they are mixed with thermal effects and modified by thermoelastic stresses. Above the breakdown threshold, the spatial confinement is partly destroyed by cavitation bubble formation, and the laser-induced effects become more disruptive. Our simulations revealed that the highly localized ablation of subcellular structures recently demonstrated by other researchers are probably mediated by free-electron-induced chemical bond breaking and not related to heating or thermoelastic stresses. At the irradiance values employed in multiphoton microscopy (≈1/20 of the breakdown threshold), the model predicts, for λ = 800 nm, an electron density of about 10^{11} cm^{-3}, sufficient to produce free electrons in the focal volume. Multiphoton microscopy may, hence, be accompanied by chemical effects arising from these electrons. We conclude that low density plasmas below the optical breakdown threshold can be a versatile tool for the manipulation of transparent biological media and other transparent materials but may also be a potential hazard in multiphoton microscopy and higher harmonic imaging.

Key words: Optical breakdown, multiphoton ionization, avalanche ionization, femtosecond pulses, photochemical effects, photothermal effects, thermoelastic stress, bubble formation, cellular laser surgery, multiphoton microscopy.

1. INTRODUCTION

Irradiance values employed in multiphoton microscopy are only a little more than one order of magnitude below the irradiance threshold for femtosecond optical breakdown in aqueous media ($\approx 1.0 \times 10^{13}$ W cm^{-2}). At the breakdown threshold, a plasma with a free electron density of about 10^{21} cm^{-3} is generated, and the energy density in the breakdown region is sufficiently high to cause the formation of a bubble at the laser focus.[1-3] We found previously that plasmas with a free electron density $<10^{21}$ cm^{-3} are formed also in a fairly large irradiance range below the breakdown threshold.[4] That raises the question of how multiphoton microscopy and higher harmonic imaging may be influenced by these "low density plasmas" and whether they can lead to cell injury.

[*] vogel@mll.mu-luebeck.de; phone: xx49-451-500-6504, fax: xx49-451-505 486; http://www.mll.mu-luebeck.de;
Medizinisches Laserzentrum Lübeck, Peter-Monnik-Weg 4, 23562 Lübeck, Germany. [§] J. Noack is now with Fresenius Medical Care

Low density plasmas with sufficiently high free-electron densities offer, on the other hand, possibilities for highly localized material processing and modification of biological media.[5-10] The topic of the present investigation is, therefore, to acquire a deeper understanding of the full potential and possible hazards of femtosecond-laser produced low-density plasmas below the optical breakdown threshold.

From an experimental point of view, the threshold for femtosecond optical breakdown is defined by the observation of bubble formation at the laser focus. From a theoretical point of view, the breakdown threshold for ultrashort pulses is usually identified with the generation of a free-electron density ρ exceeding 10^{21} cm^{-3}.[1,11,12] It is the aim of the present study to investigate the chemical, thermal, and thermomechanical effects arising from plasmas with a free electron density $\rho < 10^{21}$ cm^{-3}. We use a rate equation model considering multiphoton ionization and avalanche ionization to numerically simulate the temporal evolution of the free electron density during the laser pulse for a given irradiance, and to calculate the irradiance dependence of the free-electron density and volumetric energy density reached at the end of the laser pulse. The value of the energy density created by each laser pulse is then used to calculate the temperature distribution in the focal region after application of a single laser pulse and of series of pulses. The results of the temperature calculations yield, finally, the starting point for calculations of the thermoelastic stresses that are generated during plasma formation.

The numerical calculations are used to determine threshold values of the free-electron density and of the corresponding irradiance values above which chemical changes in the focal region, a temperature rise of 100°C, and bubble formation are expected to occur. Based on these thresholds, we discuss free-electron-mediated chemical cell damage during irradiation of whole cells with femtosecond pulses and compare the threshold values with irradiance values used for multiphoton microscopy. Finally, we discuss the ablative mechanism underlying intranuclear chromosome dissection recently demonstrated by König et al..[8] A comparison between their experimental parameters and our numerical results suggests that the chromosomal ablation is mediated by free-electron-induced chemical decomposition (bond breaking) and not related to heating or thermoelastic stresses.

2. PLASMA FORMATION

The process of plasma formation through laser-induced breakdown in transparent biological media is schematically depicted in figure 1. It essentially consists of the formation of quasi-free electrons by an interplay of multiphoton ionization and avalanche ionization.

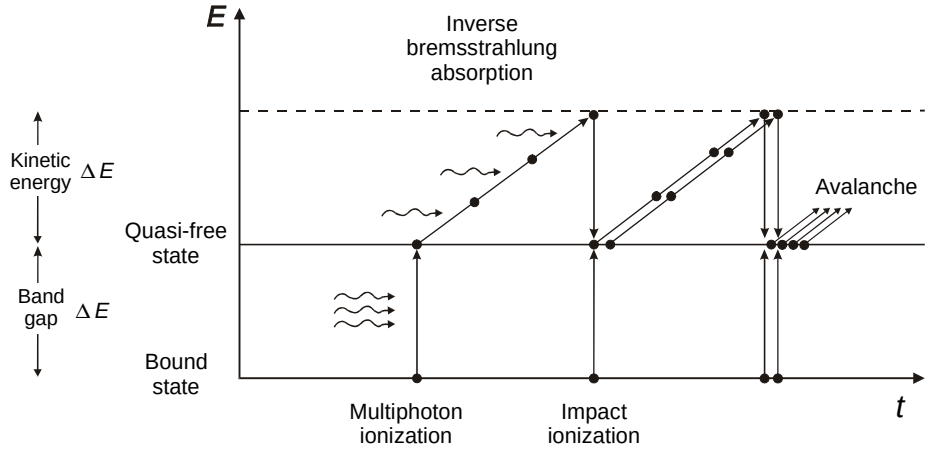

Figure 1: Interplay of multiphoton and avalanche ionization in the process of plasma formation.

It has been shown experimentally that the optical breakdown threshold in water is very similar to that in ocular and other biological media.[13] For convenience, we shall therefore focus attention on plasma formation in pure water. Whereas the optical breakdown in gases leads to the generation of free electrons and ions, it must be noted that in condensed matter electrons are either bound to a particular molecule or they are "quasi-free" if they have sufficient kinetic energy to be able to move without being captured by local potential energy barriers. Transitions between bound and quasi-free states are the equivalent of ionization of molecules in gases. To describe the breakdown process in water, Sacchi[14] has proposed that it should be treated as an amorphous semiconductor and the excitation energy ΔE regarded as the energy required for a transition from the molecular $1b_1$ orbital into an excitation band (6.5 eV).[15] We follow this approach. For simplicity, we use the terms "free electrons" and "ionization" as abbreviations for "quasi-free electrons" and "excitation into the conduction band".

The photon energies at the wavelengths of 1064 nm, 800 nm, 532 nm and 355 nm investigated in this study are 1.17 eV, 1.56 eV, 2.34 eV, and 3.51 eV, respectively. This means that the energy of six, five, three, and two photons, respectively, is required to overcome the band gap of 6.5 eV and produce an electron-hole pair. In pure water, this energy can only be provided when several photons interact simultaneously (within a time interval $\Delta t = 2\pi / \omega_L$) with a bound electron. The multiphoton ionization rate is proportional to I^k, where I is the laser light irradiance and k the number of photons required for ionization.

Once a free electron exists in the medium, it can absorb photons in a non-resonant process called 'inverse Bremsstrahlung' in the course of collisions with heavy charged particles (ions or atomic nuclei).[16] A third particle (ion/atom) is necessary for energy and momentum to be conserved during absorption, as they cannot be conserved if only an electron and a photon interact. The electron gains kinetic energy during the absorption of the photon. After a sequence of k inverse Bremsstrahlung absorption events, the kinetic energy exceeds the band gap energy ΔE. From now on, the electron can produce another free electron through impact ionization. Two free electrons with low kinetic energies are now available which can again gain energy through inverse Bremsstrahlung absorption. The recurring sequence of inverse bremsstrahlung absorption events and impact ionization leads to an avalanche growth in the number of free electrons if the irradiance is high enough to overcome the losses of free electrons through diffusion out of the focal volume and through recombination. The energy gain through inverse Bremsstrahlung must, moreover, be more rapid than the energy loss through collisions with heavy particles (a fraction of the kinetic electron energy proportional to the ratio of the electron and ion masses is transferred to the ion during each collision). The whole process is called 'avalanche ionization', or 'cascade ionization'. At very high irradiance where the losses play only a minor role, the cascade ionization rate for a given number of free electrons is proportional to the irradiance.[17]

While multiphoton ionization is "instantaneous," there are time constraints on cascade ionization because several consecutive inverse Bremsstrahlung absorption events are necessary for a free electron to pick up the kinetic energy required for impact ionization. With an ionization energy of 6.5 eV and a photon energy of, for example, 1.56 eV (corresponding to λ = 800 nm), an electron must undergo at least 5 inverse Bremsstrahlung absorption events before impact ionization can occur. As mentioned above, inverse Bremsstrahlung absorption can only occur during collisions of the electrons with heavy particles. In condensed matter, the time τ between collisions is roughly 1 fs.[18] One doubling sequence of the number of free electrons thus requires at least 5 fs, even at extremely high irradiance such that almost every collision involves inverse Bremsstrahlung absorption.

The number of free electrons produced during one laser pulse strongly depends on irradiance. In the present study, we are interested in the formation of low-density plasmas below the optical breakdown threshold. It is evident that a precise deliniation of the corresponding irradiance range requires a clear definition of the breakdown threshold. When nano- and picosecond pulses are employed, optical breakdown is accompanied by the formation of a luminous plasma and followed by shock wave emission and cavitation.[19,2] At these pulse durations, the plasma luminescence usually serves as experimental breakdown criterion.[19,5] With shorter laser pulses, there is no plasma luminescence in the visible region of the spectrum, and breakdown is experimentally detected by observing the formation of a cavitation bubble in the liquid.[11,20] In theoretical investigations, on the other hand, the breakdown threshold is defined by the irradiance (or energy) required to produce a certain critical free electron density ρ_{cr} at the laser focus. We showed previously that a good match between experimental threshold values at NA = 0.25 and theoretical predictions for optical breakdown in water is achieved assuming that the critical electron density is $\rho_{cr} = 10^{20}$ cm^{-3} for ns-pulses, and $\rho_{cr} = 10^{21}$ cm^{-3} for ps- and fs-pulses.[11] A detailed explanation of the pulse duration dependence of ρ_{cr} is given in Ref. [11].

3. NUMERICAL SIMULATIONS OF PLASMA FORMATION, TEMPERATURE EVOLUTION, AND STRESS DISTRIBUTION

3.1 Plasma formation

We first calculated the time evolution of the electron density ρ under the influence of the laser light. The time evolution of the electron plasma can, in a simplified way, be described by a rate equation of the form[11]

$$\frac{d\rho}{dt} = \eta_{\mathrm{mp}} + \eta_{\mathrm{casc}}\rho - g\rho - \eta_{\mathrm{rec}}\rho^2 . \qquad (1)$$

The first two terms represent the production of free electrons through multiphoton and cascade ionization, and the last two term describe the losses through diffusion of electrons out of the focal volume and recombination. The cascade ionization rate η_{casc} and the diffusion loss rate g are proportional to the number of already produced free electrons, while the recombination rate η_{rec} is proportional to ρ^2, as it involves an interaction between two charged particles (an electron-hole pair). A detailed description of the individual terms of Eq. (1), is given in previous publications by Kennedy,[23] and Noack and Vogel.[11]

The temporal evolution of the electron density, $\rho(t)$, was calculated for laser pulses with a Gaussian time variation,[11] focused into pure water at a numerical aperture of NA = 1.3. At least one free "seed" electron must have been produced by multiphoton ionization before cascade ionization can start (see Fig 1). Therefore, the term for cascade ionization is considered only after the free electron density owing to multiphoton ionization has increased to the point where a statistical average of 0.5 electrons exist within the focal volume. Optical breakdown should then follow with 50% probability (a certain breakdown probability has to be used as threshold criterion because optical breakdown is a statistical process. We use 50% probability in agreement with most other theoretical and experimental studies).

The focal volume was assumed to be cylindrical with a diameter equal to the focal diameter d of a Gaussian beam and a length $l = \pi d^2 / 2\lambda$ (twice the Rayleigh length). In order to account for the time $\tau_{\mathrm{ion}} = \tau k$ required for an electron to acquire the band gap energy ΔE through inverse Bremsstrahlung absorption and produce another free electron, the contribution of cascade ionization was evaluated using the electron density at time t - τ_{ion}. For our calculations, we used a value of $\tau = 1$ fs for the time between electron - heavy particle collisions.[18] To determine the irradiance threshold I_{rate} required to produce breakdown for a given wavelength and pulse duration, Eq. (1) was iteratively solved for different irradiance values until the maximum electron density during the laser pulse ρ_{max} equaled the critical density ρ_{cr} for optical breakdown. We used $\rho_{\mathrm{cr}} = 10^{20}$ cm^{-3} in the calculations referring to a pulse duration of 6 ns, and $\rho_{\mathrm{cr}} = 10^{21}$ cm^{-3} for all pulse durations in the femtosecond range.[11]

To assess the dependence of the maximum electron density on irradiance, ρ_{max} was plotted as a function of I/I_{rate}. These calculations yield the irradiance range in which low-density plasmas are produced.

Self-focusing effects can be neglected in the simulations of low-density plasma formation at a numerical aperture of NA = 1.3, even for pulse durations as short as 100 fs. The reason is that self-focusing requires a critical power to be exceeded, regardless which focusing angle is used. In contrast, optical breakdown requires an irradiance threshold to be surpassed. The power that is necessary to provide this irradiance becomes ever smaller with increasing numerical aperture and, thus, smaller spot size. Beyond a certain numerical aperture, the breakdown power is smaller than the critical power for self-focusing. Schaffer et al.[9] found that self-focusing has no influence on the breakdown threshold in water and glass for NA ≥ 0.9. It may play a role for events above the breakdown threshold, but those events are beyond the scope of this study.

3.2 Temperature distribution

The deposition of laser energy into the medium is mediated by the generation and subsequent acceleration of free electrons. The energy carried by the free electrons is then transferred to the heavy particles in the interaction volume through collisions and nonradiative recombination processes resulting in a heating of the atomic, molecular and ionic plasma constituents. To assess the time needed to establish an equilibrium temperature, we need to look at the characteristic time for electron cooling (the transfer of kinetic electron energy during collisions) and at the time scale

for recombination. The time constant for electron cooling is in the order of only a few picoseconds.[24] The recombination time can be considerably longer than this at low or moderate electron densities because the frequency of recombination events is proportional to ρ^2 (Eq. (1)). For $\rho = 10^{20}$ cm^{-3}, it takes about 40 ps until the free electron density decreases by one order of magnitude from its peak value.[11] We can conclude that for low-density plasmas it will take between a few picoseconds and tens of picoseconds until an equlibrium "thermodynamic" temperature is established.

The temperature rise can be determined by calculating the volumetric energy density gained by the plasma during the laser pulse. This calculation is particularly easy for femtosecond pulses because the pulse duration is considerably shorter than the electron cooling and recombination times. Therefore, hardly any energy is transferred during the laser pulse, and the energy density deposited into the interaction volume is simply given by the total number density ρ_{max} of the free electrons produced during the pulse multiplied by the mean energy gain of each electron. The energy gain is given by the sum of the band gap energy and the average kinetic energy of the free electrons. It is assumed in our simulations of plasma formation that every electron whose kinetic energy exceeds the band gap energy ΔE shortly produces another free electron through collisional ionization.[1,11,23] We can thus conclude that the kinetic energies in the ensemble of free electrons are between 0 and ΔE and that the mean kinetic energy is $\Delta E/2$. This yields the following simple relation for the plasma energy density ε at the end of the laser pulse:

$$\varepsilon = (3/2)\rho_{\max}\,\Delta E \tag{2}$$

The corresponding temperature rise in the interaction volume after a single laser pulse is then $\Delta T = \varepsilon / C_p$, where C_p is the heat capacity of the medium. For water, C_p =4187 J K^{-1} kg^{-1}.

The evolution of the temperature distribution within and around the interaction volume during application of a series of 100-fs pulses (λ = 800 nm) emitted at a repetition rate of 80 MHz was calculated by means of an analytic solution of the differential equations for heat diffusion. The solution is described in detail in a previous publication by Hüttmann et al..[25] The temporal shape of the laser pulses was assumed to be rectangular, and the distribution of the energy density within the plasma was assumed to be isotropic within a sphere having a volume equal to the volume of the laser focus. The actual shape of the focal volume at NA = 1.3 is ellipsoidal, with a diameter of 0.94 λ and a length of 1.38 λ. When pulses of 800 nm wavelength are focused into water, this corresponds to a diameter of 0.56 µm and a length of 0.83 µm, respectively. The radius of a sphere with equivalent volume is 0.37 µm.

3.3 Stress distribution

The temperature rise in the focal volume occurs during thermalization of the energy carried by the free electrons, i. e. within a time interval of a few picoseconds to tens of picoseconds (see section 3.2). This time interval is much shorter than the acoustic transit time from the center of the focus to its periphery which for 0.56 µm focus diameter (λ = 800 nm, NA = 1.3) is 190 ps. Therefore, no acoustic relaxation is possible during the thermalization time, and the thermoelastic stresses caused by the temperature rise stay confined in the focal volume, leading to a maximum pressure rise. The initial thermoelastic pressure at point $\boldsymbol{r}$ is given by

$$p_0(\boldsymbol{r}) = \Gamma\,\varepsilon(\boldsymbol{r}), \tag{3}$$

where ε is the volumetric energy density and Γ is the Grüneisen parameter. Paltauf and Schmidt-Kloiber[26] showed that it is a fundamental property of a photoacoustic wave emitted from a source of finite size that it must contain both compressive as well as tensile stress. It is thus possible that the rapid energy deposition results in tensile-stress-induced fracture at a temperature rise of only a few degrees Celsius, where no thermal damage can be expected.[27]

Upon plasma formation in water, the tensile part of the thermoelastic stress wave will cause the formation of a cavitation bubble when the tensile strength of the liquid is exceeded. Bubble formation is, on the other hand, the experimental criterion for optical breakdown induced by ultrashort laser pulses. Therefore, it is of great interest to correlate the values of irradiance, free-electron density, volumetric energy density, temperature rise and thermoelastic stress leading to bubble formation. When ultrashort pulses are employed for cellular surgery, it might even be possible that biomolecules are already fragmented by tensile stress amplitudes below the level required for bubble formation.

A determination of the threshold for bubble formation induced by thermoelastic stress will thus also provide a reference point for the parameter range in which thermomechanical cell damage can be expected.

To determine the evolution of the thermoelastic stress distribution in the vicinity of the laser focus, we solved the thermoelastic wave equation as described in Ref. [26]. It has to be noted that the relation (3) between deposited energy density and pressure is only linear for small temperature changes because the Grüneisen parameter depends on the temperature and thus on the energy density. The temperature dependence of Γ was taken into account using the data of Ref. [27]. Because amplitude and form of the tensile stress transient depend on the geometrical shape of the heated volume,[26] we could not assume a spherical shape as in the temperature calculations of section 3.2. The calculations were performed for an ellipsoid with a short axis of 0.56 µm and a long axis of 0.83 µm (corresponding to 800 nm radiation focused into water at NA = 1.3), assuming an isotropic distribution of energy density within this volume. We calculated the time evolution of the stress amplitude at the center of the focus, and the stress distribution along the long axis of the ellipsoid for different times after the release of the laser pulse.

4. RESULTS AND DISCUSSION

4.1 Plasma formation

The top row of figure 2 presents the evolution of the free-electron density ρ during the laser pulse at the optical breakdown threshold for 6ns, 1064 nm pulses, and for 100 fs, 532 nm pulses. To facilitate a comparison between the different pulse durations, the time t is normalized with the respective laser pulse duration τ_L. The contribution of multiphoton ionization to the total free-electron density is plotted as a dashed line. The bottom row of figure 2 shows how the maximum free electron density achieved during the laser pulse depends on irradiance.

It is obvious that the dynamics of plasma formation is extremely different for nanosecond and femtosecond pulses. With *IR nanosecond pulses*, no free electrons at all are formed for irradiance values below the breakdown threshold because the irradiance is too low to provide seed electrons by means of multiphoton ionization (Fig 2c). Once the irradiance is high enough to provide a seed electron, the ionization cascade can start. It proceeds very rapidly owing to the high irradiance (Fig. 2a). The electron density shoots up by 9 orders of magnitude within a small fraction of the laser pulse duration and even overshoots the critical electron density of $\rho_{cr} = 10^{20}$ cm^{-3}. The breakdown threshold is, hence, extremely sharp - either is a highly ionized plasma produced, or no plasma at all. It is important to note that this "sharpness" does not exclude the possibility of statistic variations of the threshold irradiance. The pulse-to-pulse variations are due to the probabilistic nature of the generation of seed electrons.

With *femtosecond pulses*, a much higher irradiance is necessary for optical breakdown to be completed during the laser pulse duration than with nanosecond pulses. This favors the generation of free electrons through multiphoton ionization because of its stronger irradiance dependence $\propto I^k$ as opposed to $\propto I$ for the cascade ionization rate (see section 2). While with nanosecond pulses the total number of free electron generated through avalanche ionization is 10^9 times larger than the number generated through multiphoton ionization (Fig. 2a), it is only 15 times larger with 100-fs pulses at 532 nm (Fig. 2b). As a consequence of the increasing importance of multiphoton ionization with shorter pulse durations, there is never a lack of seed electrons for avalanche ionization. Femtosecond-laser-induced plasma formation is, hence, a much more deterministic process than nanosecond optical breakdown. An avalanche is initiated at irradiance values considerably lower than the breakdown threshold. The free-electron density reached at the end of the avalanche depends on irradiance (Fig. 2d). Therefore, one can generated a desired free-electron density by selecting an appropriate irradiance value.

Low-density plasmas thus offer the possibility to deliberately produce chemical changes, heating, and thermomechanical effects within fairly small variations of the irradiance. These effects are very well localized because of the nonlinearity of the plasma formation process which allows to produce a plasma in a volume that is even smaller than the diffraction limited focus. The desired chemical or physical effect can be most precisely selected if the the slope of the ρ_{max} (I/I_{rate}) curve is small because that offers a large "tuning range" of the irradiance for each effect. Figure 3 shows that the tuning range increases for shorter laser wavelengths (because of the decreasing order of the multiphoton processes).

The lower end of the irradiance range for the generation of low-density plasmas reaches the range employed for multiphoton microscopy and higher harmonic imaging. To investigate potential hazards arising from these imaging modalities we shall below focus our attention on IR wavelengths which are commonly used for imaging.

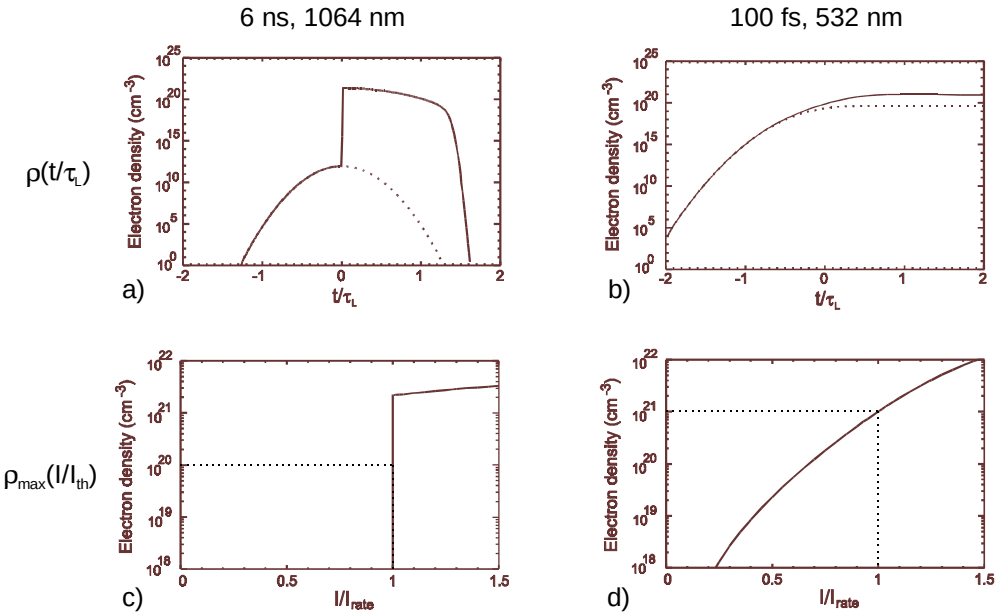

Figure 2: Top row: Evolution of the free-electron density during the laser pulse at the optical breakdown threshold for 6 ns, 1064 nm pulses and for 100 fs, 532 nm pulses. The time t is normalized with respect to the laser pulse duration τ_L. The contribution of multiphoton ionization to the total free-electron density is plotted as a dotted line. Bottom row: Maximum free electron density ρ_{max} achieved during the laser pulse as a function of irradiance, for the same laser parameters. The irradiance I is normalized with respect to the threshold irradiance I_{rate}. The threshold I_{rate} and the corresponding value of ρ_{max} are marked by dotted lines.

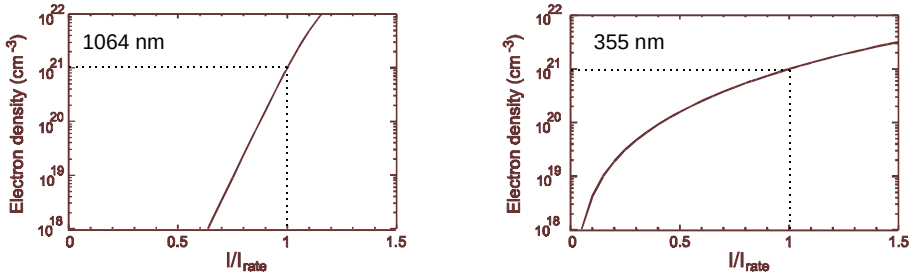

Figure 3: Maximum free electron density as a function of irradiance, ρ_{max} (I/I_{rate}), for 100 fs pulses at 1064 nm, and 355 nm wavelength. The curve for 532 nm is presented in Fig. 2d. The threshold irradiance I_{rate} and the corresponding value of ρ_{max} are marked by dotted lines.

4.2 Chemical effects induced by low-energy electrons

Plasma-mediated chemical effects in biological media can be classified into two groups: 1. Changes of the water molecules creating reactive oxygen species (ROS) which then affect organic molecules, 2. Direct changes of the organic molecules.

1. Nikogosyan et al.[28] describe the formation of OH* and H_2O_2 through various pathways following ionization and dissociation of water molecules. Both oxygen species are highly reactive and known to cause cell damage.[29] Heisterkamp et al.[30] confirmed the dissociation of water molecules during femtosecond laser-induced plasma formation by chemical analysis of the gas content of the bubbles produced at energies above the optical breakdown threshold.

2. Electrons with energies below 15 eV can initiate fragmentation of small molecules by attachment of the incident electron; this leads to the formation of a resonance, namely a transient molecular anion state[31,32] (see Fig. 4). For a molecule XY this process corresponds to $e^- + XY \rightarrow XY^{*-}$, where the XY^{*-} has a repulsive potential along the X-Y bond coordinate. The transient molecular anion state can decay by electron autodetachment (leaving a vibrationally excited molecule) or by dissociation along one, or several specific bonds such as $XY^{*-} \rightarrow X^{\bullet} + Y^-$ (Fig. 4). Boudaiffa et al.[31] describe resonant formation of DNA strand breaking induced by low-energy electrons (3-20 eV). They found that the single-strand breaks (SSB) and double-strand breaks (DSB) peak yields per incident electron are roughly one or two orders of magnitude larger than those for 10-25 eV photons. Furthermore, the ratio of DSBs to SSBs is about 1:4 for 7-20 eV electrons whereas for 10-25 eV photons it is only about 1:30.

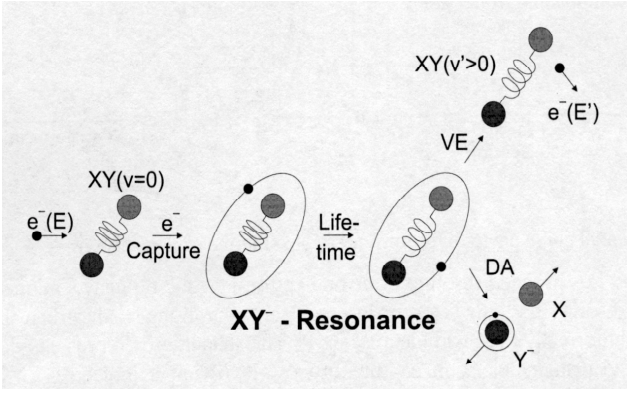

Figure 4: Dynamics of vibrational excitation (VE) and dissociative electron attachment (DA) in electron-molecule scattering through resonances (figure adapted from Hotop[32]). Resonances (compound anionic states of the electron-molecule system with lifetimes ranging typically from 10^{-15} to 10^{-11} s) often dominate the dynamics of electron-molecule collisions over the energy range 0-20 eV. A resonance is formed when the incoming electron is captured into a low-lying unoccupied molecular orbital. This attachment is allowed via an electronic transition to the state YX^{*-} only at "resonant" energies for which there is sufficient overlap between the nuclear wave functions of the initial ground state neutral and final anion states. The YX^{*-} state has typically antibonding character, i.e. the nuclei start to move to larger distances. When the electron leaves the anion after a time comparable to the average lifetime of the resonance state, the nuclei find themselves at a distance substantially larger than the equilibrium distance of the neutral molecule, i. e. in a vibrationally excited state. If the lifetime is sufficiently long to allow further propagation of the nuclei to larger distances, dissocia-tion coupled with electron attachment to one of the molecule fragments occurs (formation of $X^{\bullet} + Y^-$ or $Y^{\bullet} + X^-$).

To assess the irradiance threshold for chemical changes induced by low-density plasmas, we calculated the free-electron density as a function of irradiance for 800 nm wavelength and 170 fs pulse duration (Fig. 5). At NA = 1.3 and 800 nm wavelength, one free electron per focal volume corresponds to a density of $\rho = 4.7\times10^{12}$ cm^{-3}. Our calculations yield the result that this value is reached at an irradiance of $I = 0.55\times10^{12}$ W cm^{-2} which is 0.11 times the breakdown threshold (defined as $\rho_{cr} = 10^{21}$ cm^{-3}). Tirlapur et al.[29] experimentally observed membrane dysfunction and DNA strand breaks leading to apoptosis-like cell death after scanning irradiation of PtK2 cells with 800-nm, 90-fs pulses at 80 MHz repetition rate and 7 mW average power (total dwell time 600 µs per cell, i.e. 4.8×10^4 pulses). The average power of 7 mW corresponds to an irradiance of $I = 0.5\times10^{12}$ W/cm^{-2} which is 0.06 times the breakdown threshold, i. e. even lower than the irradiance required to produce one free electron per pulse in the focal region.

The observed damage pattern of membrane dysfunction and DNA strand breaks matches the effects which are expected to be produced by the reactive oxygen species and free electrons created during plasma formation. The damage resembles the type of injury otherwise associated with single photon aborption of UV radiation.[29] However, in

Tirlapur et al.'s experiments it arose through nonlinear absorption of NIR irradiation and the formation of a low-density plasma.

Multiphoton imaging is done with mean powers of a few milliwatts (for example, 4-8 mW with 170-fs pulses in Ref. [33]) which is fairly close to the threshold for cell damage after irradiation of whole cells reported by Tirlapur et al.[29] (7 mW with 90-fs pulses). Therefore, it cannot yet be excluded that multiphoton and higher harmonic imaging may be accompanied by chemical cell injury. It should be noted, however, that the irradiance threshold for cell injury will probably be considerably higher when *locally confined* irradiation is used to achieve knockout of individual cell organelles or intracellular dissection. Here, structures at a distance from the laser focus are efficiently protected by the strong nonlinearity of the plasma formation process.

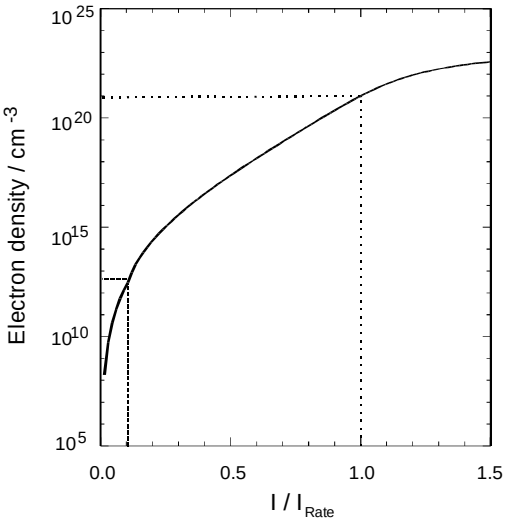

Figure 5: Maximum free electron density as a function of irradiance for 170 fs pulses at 800 nm wavelength. The threshold irradiance I_{rate} and the corresponding value of ρ_{max} are marked by a dotted line; the irradiance for which one free electron per pulse is produced in the focal volume is indicated by a dashed line.

4.3 Temperature evolution and heat effects

Figure 6 shows the calculated temperature evolution at the laser focus when a series of 800-nm, 100-fs pulses emitted at 80 MHz repetition rate is focused into water. It was assumed that an energy density of 1 J cm^{-3} is deposited per pulse. For other values of the volumetric energy density, the shape of the temperature vs time curve will be the same but the absolute values of the temperature will differ.

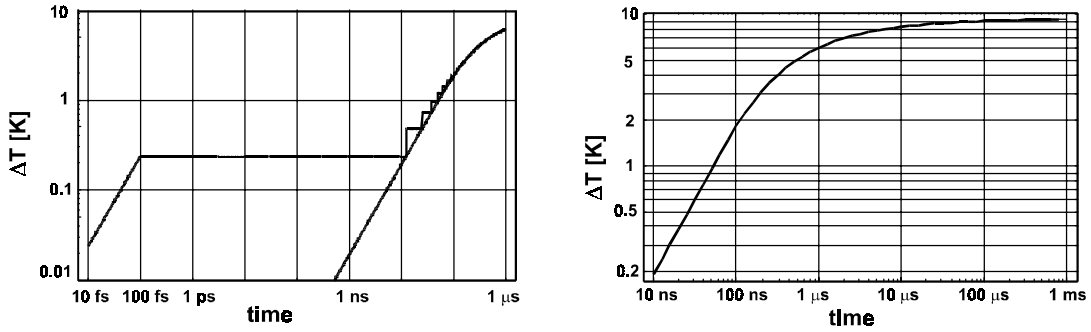

Figure 6: Temperature evolution at the laser focus produced by a series of 800 nm, 100 fs pulses emitted at 80 MHz repetition rate focused into water. The volumetric energy density deposited per pulse is 1 Jcm^{-3}. The stepwise temperature increase resulting from pulsed energy deposition exhibits a marked difference from the temperature evolution arising from cw energy deposition with the same average power (continuous line) only during the first 100 ns.

Figure 6 reveals that the total temperature increase after an irradiation time of a few microseconds is about 40 times larger than the temperature increase caused by a single pulse. This implies that fairly high peak temperatures can be produced by applying series of femtosecond pulses with energies well below the breakdown threshold.

Starting from room temperature, 100°C are reached when each individual pulse produces a temperature rise of 2°C. This temperature rise requires a free-electron density of $\rho = 7.3\times10^{18}$ cm^{-3}, which amounts to 0.73% of the critical density of $\rho_{cr} = 10^{21}$ cm^{-3} serving as threshold criterion for optical breakdown. The corresponding irradiance for 800-nm, 170-fs pulses is $I = 3.3\times10^{12}$ W/cm^{-2} which is 0.66 times the irradiance value required for optical breakdown. At 355 nm, a temperature of 100°C can be reached with an irradiance of only 0.12 times the breakdown threshold. The irradiance range in which thermal effects below the optical breakdown threshold are produced is, hence, considerably broader for shorter wavelengths.

The calculated temperature distribution in the vicinity of the laser focus for different times after the start of a fs-pulse series focused at NA = 1.3 is plotted in figure 7. It is remarkable that the temperature distribution remains fairly narrow even after a few microseconds when a dynamic equilibrium between energy deposition and heat diffusion has been established. The rapid decrease of the temperature with increasing distance from the laser focus is related to the spherical shape of the focal volume which allows for heat diffusion in all directions.

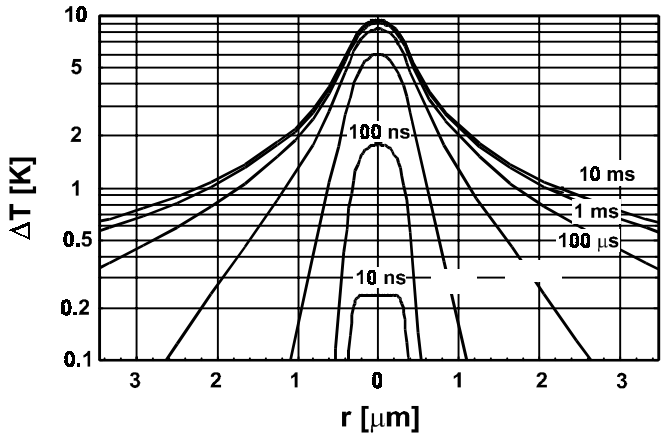

Figure 7: Temperature distribution in the vicinity of the laser focus produced by series of 800-nm, 100-fs pulses emitted at 80 MHz repetition rate that are focused into water. The volumetric energy density deposited per pulse is 1 J cm^{-3}.

The results of our temperature calculations suggest, at first sight, that an irradiance range below the optical breakdown threshold exists where purely thermal effects in biological media can be produced. However, one needs to consider that more than 10^6 free electrons per pulse are generated in the focal volume at the irradiance which creates a temperature difference of 2°C per pulse and a peak temperature of 100°C after a pulse series of several microseconds. Any thermal denaturation of biomolecules will thus always be mixed with free-electron-induced chemical effects, and the latter will probably dominate. In section 4.4 we shall see that the heat effects are also mixed with the generation of strong thermoelastic stresses.

4.4. Evolution of the stress distribution, and bubble formation

The thermalization time of the energy carried by the free electrons (a few picoseconds to tens of picoseconds, see section 3.2) is much shorter than the acoustic relaxation time for the focal volume (190 ps when laser pulses of 800 nm wavelength are focused into water at NA = 1.3, see section 3.3). The energy deposition occurs, hence, under stress confinement conditions. The degree of stress confinement tp* is given by the ratio of thermalization time over acoustic relaxation time. For femtosecond pulses, it is ≤ 0.1.

Stress confinement results in the generation of strong thermoelastic stress waves. Figure 8 shows the spatial stress distribution for various points in time after the release of the laser pulse, and figure 9 presents the temporal evolution of the stress amplitude in the center of the focal volume.

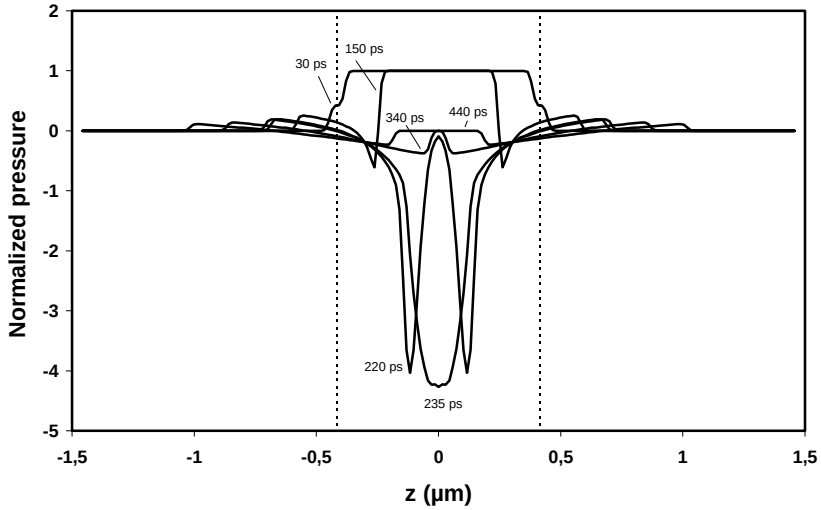

Figure 8: Stress distribution in the vicinity of the laser focus produced by a single femtosecond pulse focused into water, for various points in time after the release of the laser pulse. The calculations were performed for an ellipsoid with a short axis of 0.56 µm and a long axis of 0.83 µm (corresponding to 800 nm radiation focused into water at NA = 1.3), assuming an isotropic distribution of energy density within this volume. The thermalisation time of the energy carried by the free electrons was assumed to be 20 ps. The corresponding value of the degree t_p* of stress confinement (thermalization time divided by acoustic relaxation time) is t_p* = 0.105. The pressure amplitudes are normalized to the peak compressive stress created in the focal volume. The dashed lines represent the extension of the ellipsoidal focal volume along the optical axis (beam waist at z = 0). The absolute values of the pressure amplitude are related to the plasma energy density according to Eq. (3).

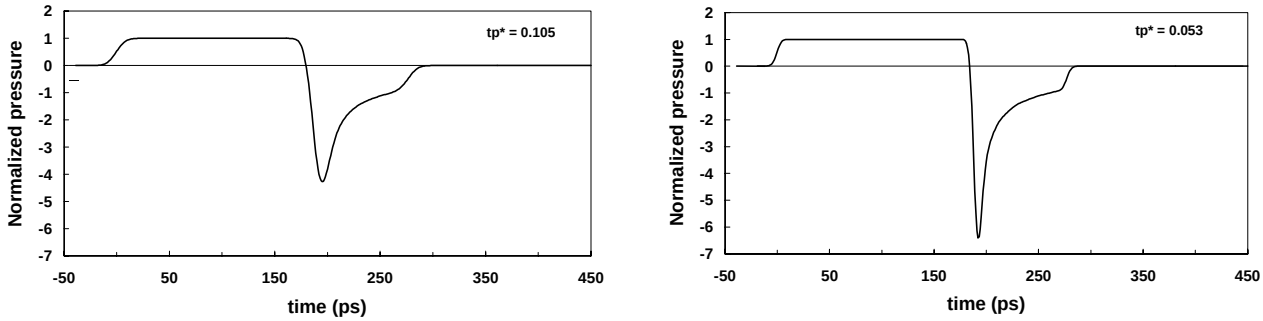

Figure 9: Temporal evolution of the stress amplitude in the center of the focal volume after a single 800-nm femtosecond pulse focused into water. Calculations were performed for thermalization times of 20 ps (a) and 10 ps (b), corresponding to t_p* = 0.105 and t_p* = 0.053, respectively. The "thermalization pulses" were assumed to have a Gaussian temporal shape, with the peak at t = 0.

The thermoelastic expansion of the focal volume produces a compressive wave traveling into the surrounding medium. The amplitude of the compressive wave just outside the heated volume amounts to 0.5 times the value inside that volume, and at larger distances r it decreases proportional to 1/r (of even faster if the pressure is high enough for a shock front to be formed[2]). When the thermal expansion comes to a rest, inertial forces lead to the generation of a tensile stress wave that propagates from the periphery of the focal volume into its center and is focused in the center of symmetry. Because of the focusing, the peak tensile stress amplitudes are 4 to 6 times higher than the peak compressive amplitudes.

The peak tensile stress amplitude depends on three factors: 1. the shape of the heated volume (the tensile stress can be up to 20 times higher than the compressive stress when the shape is spherical and $tp^* \leq 0.05$ [26]), 2. the degree of stress confinement, and 3. the temperature distribution within the heated volume. A temperature distribution with sharp edges results in a short tensile stress wave with very high amplitudes. The assumption of a homogeneous temperature distribution with sharp edges made in our calculations will thus yield unrealistically high values of the tensile stress wave if not compensated for. A compensation is provided by our assumption of a Gaussian temporal shape for the "thermalization pulse". In reality, this pulse is exponential with an ultrashort rise time equal to the laser pulse duration and a longer decay governed by the energy transfer through collisions and recombination. The assumption of a Gaussian thermalization pulse leads to a smoothening of the predicted shape of the tensile stress wave and to a lowering of its amplitude and thus to a similar outcome as a realistic temperature distribution with smooth borders.

The tensile stress results in the formation of a cavitation bubble if it exceeds the tensile strength of water. Because the focal volume is very small (≈0.2 μm^3) and the region subjested to tensile stress is even smaller (Fig.8), no nuclei will be present which could facilitate bubble formation. Therefore, we have to consider the tensile strength of pure water. It is about -275 bar for a stress wave duration of 1 µs,[34] and we estimate that it will be about -300 bar for stress wave durations in the picosecond range. Generation of a tensile stress of -300 bar requires a temperature rise of 11°C when the thermalisation time is 10 ps, and of 16.5°C when it is 20 ps.

A temperature increase of 11°C is produced by a a free-electron density of $\rho = 0.4\times10^{20}$ cm^{-3}. This is less than the optical breakdown criterion of $\rho_{cr} = 10^{21}$ cm^{-3} assumed in most theoretical studies. The irradiance value corresponding to bubble formation is $I = 0.81\times I_{th}$ for a wavelength of 800 nm, and $I = 0.27\times I_{th}$ for 355 nm, whereby I_{th} refers to the threshold criterion $\rho_{cr} = 10^{21}$ cm^{-3}. This discrepancy needs to be kept in mind when comparing the results of experimental studies, where bubble formation serves s breakdown criterion, with those of numerical simulations.

We can conclude that with laser pulse durations in the femtosecond and lower picosecond range very high compressive and tensile stress amplitudes are created already by a moderate temperature increase at the laser focus. The stress produced by a temperature rise of about 10-15°C results in the formation of a cavitation bubble in pure water. The situation is very different for longer pulse durations where the stress confinement condition is not fulfilled. For pulses considerably longer than the thermalization time of the free-electron energy, large amounts of energy are transferred from the free electrons to the heavy particles during the laser pulse.[11] This leads to a high value of the plasma energy density and a temperature of several thousand degrees Kelvin,[1,35] which, in turn, drives the emission of a shock wave.[1,2]

4.5 Mechanism of intracellular ablation and dissection

König and coworkers have recently reported intranuclear and extracellular chromosome dissection using high repetition-rate trains of NIR femtosecond laser pulses focused at high numerical aperture.[8,33] A complete dissection of extracellular chromosomes could be performed with an FWHM cut size of 1/3 of the diffraction limitated focal spot size. The present study, to our knowledge, allows for the first time to identify the working mechanism of the intracellular and extracellular ablation.

For this purpose, the results of the previous sections are summarized in figure 10. The different low-density plasma effects and breakdown phenomena are listed together with the corresponding values of free-electron density and irradiance. Within this framework we have also plotted the physical parameters used for intranuclear chromosome dissection (our model simulates the plasma formation in the bulk of aqueous media, and cannot, without further considerations, be applied to chromosome dissection in air). The laser parameters employed by König et al.[8] were: 170-fs pulse duration, 800 nm wavelength, 80 MHz repetition rate, 30 mW average power, 0.5 ms dwell time at the chromosome, NA = 1.3. This corresponds to an irradiance of 0.9×10^{12} Wcm^{-2} ($I = 0.17 \times I_{th}$) which leads to a free-electron density of $\rho = 2\times10^{14}$ cm^{-3}. This free-electron density gives rise to a thermoelastic tensile stress of $\approx10^{-3}$ bar after each pulse, and to a temperature increase of $\approx10^{-3}$°C after a pulse series of 1 µs duration.

The stress and the temperature rise induced by the low-density plasmas are by far too small to cause any cutting effect or other types of cell injury. Therefore, it is very likely that the intracellular ablation produced by trains of femtosecond pulses relies on cumulative chemical effects. Breaking of chemical bonds by low-energy electrons, as described in section 4.2, may lead to a disintegration of the structural integrity of biomolecules and finally to a dissection of subcellular structures.

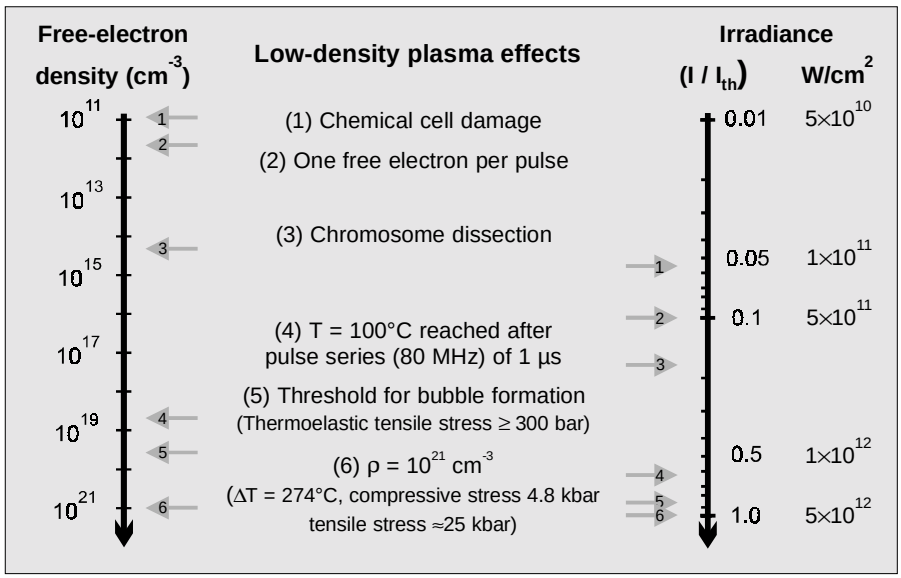

Figure 10: Overall view of low-density plasma effects and breakdown phenomena induced by femtosecond laser pulses. The different effects are depicted together with the corresponding values of free-electron density and irradiance. The irradiance values are given both in absolute terms (W/cm^2), and normalized to the otpical breakdown threshold I_{th} defined by a critical electron density of $\rho_{cr} = 10^{21}$ cm^{-3}. All data refer to plasma formation in water with 170-fs pulses at 800 nm wavelength.

4. CONCLUSIONS

We investigated the effects induced by femtosecond laser-generated low-density plasmas at irradiance values below the optical breakdown threshold. The investigations were based on numerical simulations of plasma formation yielding the temporal evolution of the free electron density during the laser pulse and the volumetric energy density at the end of the pulse. The value of the energy density created by each laser pulse was then used to calculate the temporal evolution of the temperature distribution and of the thermoelastic stress distribution in the focal region.

The accuracy of all results depends on the validity of the model used for the simulation of plasma formation. In a previous study on laser-induced breakdown in water at nanosecond to femtosecond time scales[11], we found very good agreement between the breakdown thresholds determined experimentally at a numerical aperture of NA ≈ 0.25 and the values obtained by numerical simulations for the same NA. Therefore, we are optimistic that the results obtained in the present study for plasma formation at NA = 1.3 constitute a reasonable basis for the subsequent calculations of temperature and stress distributions, and for the discussion of recent experimental results obtained by other researchers.

Femtosecond laser pulses create spatially extremely confined chemical, thermal and mechanical effects via free-electron generation through nonlinear absorption. Photochemical effects dominate at the lower end of this irradiance range, whereas at the upper end they are mixed with thermal effects and modified by thermoelastic stresses. Above the breakdown threshold, the spatial confinement is partly destroyed by cavitation bubble formation, and the laser-induced effects become more disruptive. Our simulations revealed that the highly localized ablation of intracellular structures and intranuclear chromosome dissection recently demonstrated by other researchers are probably mediated by free-electron-induced chemical bond breaking and not related to heating or thermoelastic stresses.

A matter of concern is that low-density plasmas could be a potential hazard in multiphoton microscopy and higher harmonic imaging. Multiphoton imaging is done with mean powers of a few milliwatts (for example, 4-8 mW with 170-fs pulses in Ref. [33]) which is fairly close to the threshold for cell damage during *irradiation of whole cells* reported by Tirlapur et al.[29] (7 mW with 90-fs pulses).

The irradiance threshold for cell injury will probably be considerably higher when *locally confined irradiation* is used to achieve knockout of individual cell organelles or intracellular dissection. Here, structures at a distance from the laser focus are efficiently protected by the strong nonlinearity of the plasma formation process. Low density plasmas below the optical breakdown threshold are, therefore, a versatile tool for the manipulation of transparent biological media. Effect sizes below the diffraction limit can be reached because of the nonlinear nature of plasma formation. Short wavelengths seem to be best suited for the manipulation of cellular events because they enable a particularly fine tuning between chemical, thermal and mechanical effects due to the relatively weak dependence of the free-electron density on irradiance. Short wavelengths in the visible or UVA portion of the optical spectrum, provide, furthermore, a much better spatial resolution than infrared wavelengths.

REFERENCES

1. A. Vogel: *Optical Breakdown in Water and Ocular Media and its Use for Intraocular Photodisruption*, Shaker, Aachen, 2001.
2. A. Vogel, S. Busch, and U. Parlitz, "Shock wave emission and cavitation bubble generation by picosecond and nanosecond optical breakdown in water," *J. Acoust. Soc. Am.* **100**, 148-165, 1996.
3. A. Vogel, J. Noack, K. Nahen, D. Theisen, S. Busch, U. Parlitz, D. X. Hammer, G. D. Nojin, B. A. Rockwell, and R. Birngruber, "Energy balance of optical breakdown in water at nanosecond to femtosecond time scales," *Appl. Phys. B* **68**, 271-280, 1999.
4. A. Vogel and J. Noack, " Numerical simulation of optical breakdown for cellular surgery at nanosecond to femtosecond time scales," *Proc. SPIE* **4260**, 83-93, 2001.
5. V. Venugopalan, A. Guerra, K. Nahen, A. Vogel, "The role of laser-induced plasma formation in pulsed cellular microsurgery and micromanipulation," *Phys. Rev. Lett.* **88(7)** 078103(1-4), 2002.
6. M. W. Berns, W. H. Wright, R. Wiegand-Steubing, "Laser-microbeams as a tool in cell biology," *Int. Rev. Cytol.* **129**, 1-44, 1991.
7. Schütze K, Pösl H and Lahr G, "Laser micromanipulation systems as universal tools in molecular biology and medicine," Cell. Mol. Biol. **44**: 735-746, 1998.
8. K. König, I. Riemann, P. Fischer, and K. Halbhuber, "Intracellular nanosurgery with near infrared femtosecond laser pulses," *Cell. Mol. Biol.* **45**, 195-201, 1999.
9. C. B. Schaffer, A. Brodeur, J. F. García, and E. Mazur, "Micromachining bulk glass by use of femtosecond laser pulses with nanojoule energy," *Opt. Lett.* **26**, 93-95, 2001.
10. K. Minoshima, A. M. Kowalevicz, I. Hartl, E. Ippen, J. G. Fujimoto, "Photonic device fabrication in glass by use of nonlinear materials processing with a femtosecond laser oscillator," *Opt. Lett*. **26,** 1516-1518, 2001.
11. J. Noack and A. Vogel, "Laser-induced plasma formation in water at nanosecond to femtosecond time scales: Calculation of thresholds, absorption coefficients, and energy density," *IEEE J. Quantum Electron.* **35**, 1156-1167, 1999.
12. B. C. Stuart, M. D. Feit, S. Hermann, A. M. Rubenchik, B. W. Shore, and M. D. Perry, "Nanosecond to femto-second laser-induced breakdown in dielectrics," *Phys. Rev. B* **53**, 1749-1761, 1996.
13. F. Docchio, C. A. Sachhi, and J. Marshall, "Experimental investigation of optical breakdown thresholds in ocular media under single pulse irradiation with different pulse durations," *Lasers Ophthalmol*. **1**, 83-93, 1986.
14. C. A. Sacchi, "Laser-induced electric breakdown in water," *J. Opt. Soc. Am. B*. **8**, 337-345, 1991.
15. F. Williams, S. P., Varama, and S. Hillenius, "Liquid water as a lone-pair amorphous semiconductor," *J. Chem. Phys.* **64**, 1549-1554, 1976.
16. J. F. Ready, *Effects of High Power Laser Radiation,* Academic Press, Orlando, 1971, pp. 261-262.
17. Y. R. Shen, *The Principles of Nonlinear Optics*, Wiley, New York, 1984.
18. N. Bloembergen, "Laser-induced electric breakdown in solids," *IEEE J. Quantum Electr.* **QE-10**, 375-386, 1974.

19. A. Vogel, K. Nahen, and D. Theisen, "Plasma formation in water by picosecond and nanosecond Nd:YAG laser pulses - Part I: Optical breakdown at threshold and superthreshold irradiance," *IEEE J. Selected Topics Quantum Electron.* **2**(4), 847-860, 1996.

20. D. X. Hammer, R. J. Thomas, G. D. Noojin, B. A. Rockwell, P. A. Kennedy, and W. P. Roach, "Experimental investigation of ultrashort pulse laser-induced breakdown thresholds in aqueous media," *IEEE J. Quantum Electr.* **QE-3**, 670-678, 1996.

21. M. Lenzner, J. Krüger, S. Sartania, Z. Cheng, Ch.Spielmann, G. Mourou, W. Kautek, and F. Krausz, "Femtosecond optical breakdown in dielectrica," *Phys. Rev. Lett.* **80**, 4076-4079, 1998.

22. M. Bass (ed in chief), Opt. Soc. Am., *"Handbook of Optics Vol. II,"* McGraw Hill, New York, 1995.

23. P. K. Kennedy, "A first-order model for computation of laser-induced breakdown thresholds in ocular and aqueous media: Part I - Theory," *IEEE J. Quantum Electron.* **QE-31**, 2241-2249, 1995.

24. S. Nolte, Cl. Momma, H. Jacobs, A. Tünnermann, B.N.Chikov, B. Wellegehausen, and H. Welling, " Ablation of metals by ultrashort laser pulses," *J. Opt. Soc. Am. B* **14**, 2716-2722, 1997.

25. G. Hüttmann, J. Serbin, B. Radt, B. Lange, and R. Birngruber, "Model system for investigating laser-induced subcellular microeffects," *Proc. SPIE* **4257**, 398-409, 2001.

26. G. Paltauf and H. Schmidt-Kloiber, "Photoacoustic cavitation in spherical and cylindrical absorbers," Appl. Phys. A **68**, 525-531, 1999.

27. G. Paltauf and H. Schmidt-Kloiber, "Microcavity dynamics during lasr-induced spallation of liquids and gels," Appl. Phys. A **62**, 303-311, 1996.

28. D. N. Nikogosyan, A. A. Oraevsky, and V. Rupasov, "Two-photon ionization and dissociation of liquid water by powerful laser UV radiation," *Chem. Phys.* **77**, 131-143, 1983.

29. U. K. Tirlapur, K. König, C. Peuckert, R. Krieg, and K.-J. Halbhuber, "Femtosecond near-infrared laser pulses elicit generation of reactive oxygen species in mammalian cells leading to apoptosis-like death," *Exp. Cell Res.* **263**, 88-97, 2001.

30. A. Heisterkamp, T. Ripken, H. Lubatschowski, T. Mamom, W. Drommer, H. Welling, W. Ertmer, " Nonlinear side-effects of fs-pulses inside corneal tissue during photodisruption," *Appl. Phys. B* **74**, 2002 (in press).

31. B. Boudaiffa, P. Cloutier, D. Hunting, M. A. Huels, L. Sanche, "Resonant formation of DNA strand breaks by low-energy (3 to 20 eV) electrons," *Science* **287**, 1658-1660, 2000.

32. H. Hotop, "Dynamics of low energy electron collisions with molecules and clusters," in *Proc. Int. Symp. on Gaseous Dielectrics IX 22-25 May 2001, Ellicott City, MD, USA*, L.G. Christophorou, J.K. Olthoff (Eds.) Kluwer Academic/Plenum Press, pp. 3-14, 2001.

33. K. König, I. Riemann, W. Fritsche, "Nanodissection of human chromosomes with near-infrared femtosecond laser pulses," *Opt. Lett.* **26**, 819-821, 2001.

34. H.-Y. Kwak and R.L. Panton, "Tensile strength of simple liquids predicted by a model of molecular interactions," *J. Phys. D: Appl. Phys.* **18**, 647-659, 1985.

35. E. J. Chapyak, R. P. Godwin, and A. Vogel, "A comparison of numerical simulations and laboratory studies of shock waves and cavitation bubble growth produced by optical breakdown in water," *Proc. SPIE* **2975**, 335-342, 1997.